Journal of Power Sources 194 (2009) 303–312

Contents lists available at ScienceDirect

Journal of Power Sources

journal homepage: www.elsevier.com/locate/jpowsour

A stochastic geometry based model for total triple phase boundary length in composite cathodes for solid oxide fuel cells

A.M. Gokhale*, S. Zhang, M. Liu

School of Materials Science and Engineering, Georgia Institute of Technology, Atlanta, GA, United States

ARTICLE INFO

Article history:
Received 10 April 2009
Received in revised form 7 May 2009
Accepted 8 May 2009
Available online 20 May 2009

Keywords:
Triple phase boundary length
Composite cathodes
SOFC
Cermet
Microstructure

ABSTRACT

An analytical equation is derived for total triple phase boundary length per unit volume (L_{TPB}) in an isotropic uniform random microstructure of LSM/YSZ composite cathode. The equation is applicable to YSZ and LSM particles of any convex shapes and size distributions. The equation explicitly relates L_{TPB} to the shapes, mean sizes, coefficient of variation (a measure of the spread in a size distribution) and skewness of YSZ and LSM particle populations, and volume fractions of YSZ, LSM, and porosity. The equation is verified using available experimental data, and compared with the results of earlier simulations and models. The parametric analysis reveals that (1) non-equiaxed plate-like, flake-like, and needle-like YSZ and LSM particle shapes can yield substantially higher L_{TPB}; (2) mono-sized YSZ and LSM powders lead to higher L_{TPB} as compared to the powders having size distributions with large coefficient of variation; (3) L_{TPB} is inversely proportional to the mean sizes of YSZ and LSM particles; (4) high value of L_{TPB} is obtained at the lowest porosity volume fraction that permits sufficient connectivity of the pores for gas permeability; and (5) L_{TPB} is not sensitive to the relative proportion of YSZ and LSM phases in the regime of interest in composite cathode applications.

1. Introduction and background

The need for clean and sustainable energy has stimulated great interest in fuel cells. The advantages of solid oxide fuel cells (SOFCs) over other types of fuel cells include high energy efficiency and excellent fuel flexibility [1,2]. A wide variety of fuels can be directly utilized in SOFCs, including hydrocarbon fuels, coal gas, and renewable fuels. To be economically competitive and commercially viable, however, the performance of SOFCs must be further improved and the cost must be reduced. The performance of SOFCs is often limited by the *interfacial losses* arising from the resistances to charge and mass transfer along surfaces; across interfaces; and through the porous electrodes, especially through the cathode where oxygen reduction takes place [3]. Lanthanum doped strontium manganite (LSM) is the most widely used cathode for SOFC based on yttria-stabilized zirconia (YSZ) electrolyte because of its excellent chemical and thermal compatibility with YSZ. Nonetheless, the catalytic activity of LSM is severely limited by its poor ionic conductivity, particularly at low operating temperatures. Consequently, in the LSM/YSZ cathodes, the electrochemically active sites for oxygen reduction reactions are mostly at the triple phase boundaries (TPB), which are the lineal regions common to LSM, YSZ, and air. Therefore, an important strategy to increase the catalytic activity in the cathodes at low temperatures is to increase the number of such active sites via an increase in the total length of the TPB per unit volume of microstructure (L_{TPB}) through rational design of porous composites containing LSM and YSZ [4–7]. The performance of such composite cathodes is microstructure sensitive [8–12].

The LSM/YSZ composite cathodes are typically fabricated using powder processing techniques involving printing or spraying and sintering of a powder mix consisting of YSZ and LSM powders. It has been reported that the microstructure of the composite cathodes is sensitive to the processing parameters such as the mean sizes of the initial powders [10,11] and sintering temperature [9,12]. The microstructure in turn affects the performance of the cathode. One of the key microstructural parameters that affects the electro-chemical response of porous LSM/YSZ cathodes is the total length of the LSM-YSZ-porosity triple phase boundaries in the three-dimensional (3D) microstructure per unit volume (i.e., L_{TPB}) because O_2 reduction and incorporation of O^{2-} into the electrolyte take place at these sites [8]. Accordingly, development of quantitative relationships among the processing parameters, microstructural geometry, and electro-chemical response of composite cathode materials is vital to the effective optimization of electrode performance. Therefore, it is of interest to develop the quantitative relationships that describe the effects of the process variables such as morphology, mean sizes and size distributions of the powders of YSZ and LSM prior to sintering on L_{TPB}.

* Corresponding author. Tel.: +1 404 894 2887; fax: +1 404 894 9140.
E-mail address: arun.gokhale@mse.gatech.edu (A.M. Gokhale).

0378-7753/$ – see front matter © 2009 Elsevier B.V. All rights reserved.
doi:10.1016/j.jpowsour.2009.05.012

The relationships between L_{TPB} and the geometric characteristic of the powder mix prior to sintering have been studied via geometric computer simulations of the composite cathode microstructure [13–21]. Such simulated microstructures are also useful for implementation in the computational simulations of the electrochemical behavior and performance of the composite cathode [13,14,16–21]. The microstructure simulations must allow overlaps among the YSZ and LSM particles to create the TPB because simulations based on non-overlapping particles (so called hard-core simulations) contain only point contacts among the particles. Consequently, the simulated L_{TPB} depends on the extent of the overlaps permitted. Geometric simulations of L_{TPB} reported in the literature can be divided into two groups: (a) the simulations where the YSZ and LSM particles are placed on a periodic lattice but the lattice points are occupied by either YSZ or LSM in a random fashion with the probability proportional to their respective number densities [13,14,16,20], and (b) the simulations involving random packing of impenetrable mono-sized spheres of YSZ and LSM followed by a fixed amount of dilation (increase) of sphere diameters to create particle overlaps and TPB [15,17,18,21]. The stochastic nature of the spatial distribution of the particle centers in the real microstructure of the composite cathode is not captured in the simulations based on a periodic lattice (i.e., group (a)), whereas the simulations based on random packing of YSZ and LSM particles account for the stochastic nature of the corresponding real microstructures. Earlier simulations of the TPB assume that the YSZ and LSM particles are spherical and mono-sized. On the other hand, in a typical powder mix, *distributions* of sizes of YSZ and LSM particles usually exist. Thus, the simulations do not reveal the effects of the particle shape and the distribution attributes such as the variance and the skewness of the particle sizes on the L_{TPB}.

Analytical models have also been proposed for L_{TPB} [17,20]. These models assume that (i) YSZ and LSM particles are spherical and mono-sized, (ii) all TPB are of the same length, and (iii) there is no distribution of coordination numbers present in the microstructure. To compute L_{TPB} using these models, it is essential to know the mean coordination number for the particle populations, which cannot be measured experimentally, except via reconstruction of the 3D microstructure [22], and is difficult to compute from theoretical considerations without making numerous simplifying assumptions. Further, a distribution of coordination numbers usually exists in the real microstructures having a distribution of particle sizes, and there is often a strong correlation between the particle size and the coordination number: larger particles have higher coordination numbers [22]. In this contribution, a stochastic geometry [23–25] based equation is derived that relates L_{TPB} in the 3D microstructure of the composite cathode to the parameters such as particle shape/morphology; mean sizes, standard deviation and skewness of YSZ and LSM size distributions; relative amounts of YSZ and LSM; and volume fraction of the porosity. The equation is based on a well-known stereological relationship for estimation of microstructural surface area in 3D microstructures [26–28]. The derivation of the equation is presented in the next section, and that is followed by critical analysis of the model, comparison with experimental data, and parametric studies for microstructural engineering to optimize L_{TPB}.

2. Theoretical development

2.1. Extended microstructure

Consider a geometric microstructure model comprising an isotropic uniform random (IUR) collection of convex[1] particles of YSZ and LSM in a 3D microstructural space, where the spatial arrangement of the particle centers is given by the Poisson process of spatial statistics [29], and the particles are allowed to freely intersect and overlap with one another depending on their spatial locations. Assume that there are no spatial correlations in the locations of the particles. The space not occupied by YSZ and/or LSM phases is the porosity. Such a geometric microstructure model is called an "extended" microstructure; the concept is widely used in modeling phase transformations [30–35]. The classical Johnson–Mehl–Avrami equation used in phase transformation theories [30–32] utilizes the concept of "extended" microstructure. The concept of "extended" microstructure was initially developed for two-phase microstructures, but recently it has been modified to model microstructures containing three or more phases [33–35].

Clearly, in a real microstructure the particles cannot overlap. Therefore, the properties of an extended microstructure (such as volume fractions of phases) are overestimates of the properties of the corresponding "real" microstructure. Nonetheless, the "real" microstructure model (i.e., microstructure model for composite cathode) can be recovered from the corresponding extended microstructure by subtracting the overlapped regions from it. Mathematically, each convex particle in an extended microstructure can be considered as a convex set, and an extended microstructure can be treated as an IUR ensemble of convex sets. Therefore, the corresponding "real" microstructure is simply the *union* of these convex sets, which is amenable to an analytical treatment using Boolean algebra of convex sets [36]. The microstructural properties of the corresponding "real" microstructure obtained by subtracting the overlapped regions in the extended microstructure can be computed analytically from the properties of the extended microstructure [36–38]. Let $(\theta_Y)_{ex}$ and $(\theta_L)_{ex}$ be the volume fractions of YSZ and LSM in our extended microstructure. As the particles of YSZ and LSM are allowed to overlap in the extended microstructure, $(\theta_Y)_{ex}$ and $(\theta_L)_{ex}$ are not *equal to* their volume fractions θ_Y and θ_L in the corresponding real microstructure, but they are related as follows [33–35].

$$(1+\alpha)\theta_L = 1 - \exp\{-(1+\alpha)(\theta_L)_{ex}\} \tag{1}$$

$$\frac{\alpha+1}{\alpha}\theta_Y = 1 - \exp\left\{-\frac{1+a}{\alpha}(\theta_Y)_{ex}\right\} \tag{2}$$

where,

$$\frac{\theta_Y}{\theta_L} = \frac{(\theta_Y)_{ex}}{(\theta_L)_{ex}} = \alpha \tag{3}$$

The parameter α is the relative proportion of YSZ and LSM phases in the microstructure. In a microstructure containing YSZ, LSM, and porosity, the sum of the *real* volume fractions of YSZ, LSM, and porosity must be equal to one[2]. Therefore,

$$\theta_Y + \theta_L + \theta_P = 1 \tag{4}$$

In Eq. (4), θ_P is the volume fraction of the porosity in the real microstructure. Combining Eqs. (1)–(4) leads to the following equation for the product of the extended volume fractions of YSZ and LSM. This key equation will be needed subsequently.

$$(\theta_Y)_{ex}(\theta_L)_{ex} = \frac{\alpha}{(1+\alpha)^2}[\ln(\theta_P)]^2 \tag{5}$$

[1] A particle shape is convex if a line joining any (and all) two arbitrary points on its surface lies inside the particle. Spheres, ellipsoids, polyhedrons with flat faces, cylinders, cones, plates, needles, etc. are all convex.

[2] Note that in the present work, the volume fraction of a phase is equal to the total volume occupied by that phase in the microstructural space divided by the total volume of the microstrucutral space (i.e., specimen volume). This definition is different from the one used in the earlier papers on modeling of cathode microstructure [15,17,42].

2.2. Relationship between triple phase boundary lengths in real and extended microstructures

In the extended microstructure, the YSZ and LSM particles are permitted to overlap and intersect. The lines of intersection of the YSZ and LSM particles are the lineal regions common to YSZ, LSM, and porosity, and therefore, they are the TPB of interest in the *extended* microstructure. Let $(L_{TPB})_{ex}$ be the total length of these lines of intersection in the *extended* microstructure per unit volume, and let L_{TPB} be their total length in the corresponding *real* microstructure per unit volume. In general, L_{TPB} is not equal to $(L_{TPB})_{ex}$ because not all segments of the TPB in the extended microstructure contribute to the L_{TPB} in the real microstructure: only those triple phase boundary line segments are present in the real microstructure that are *not* located in the space already occupied by other YSZ and/or LSM particles, i.e., those that are located in the space occupied by the porosity. In an IUR microstructure, the probability that a randomly located infinitesimal line element falls in the porosity phase is precisely equal to the volume fraction of the porosity [23–28], and the probability is the same for all such line elements and independent of the location. Therefore, the fraction of the total length of the TPB in the extended microstructure that is present in the corresponding real microstructure, $L_{TPB}/(L_{TPB})_{ex}$, is precisely equal to the volume fraction of the porosity phase, θ_P, i.e.,

$$\frac{L_{TPB}}{(L_{TPB})_{ex}} = \theta_P \tag{6}$$

or,

$$L_{TPB} = (L_{TPB})_{ex}\theta_P \tag{7}$$

It remains to derive an expression for $(L_{TPB})_{ex}$ in terms of the geometric characteristics of YSZ and LSM particles to complete the derivation.

2.3. Relationship between L_{TPB} and geometric attributes of YSZ, LSM, and porosity

Numerous geometric attributes of 3D microstructures can be statistically estimated from the measurements performed on lower dimensional manifolds such as random two-dimensional (2D) sections through the 3D microstructure using classical stereological relationships [23–28]. For example, volume fractions of the phases, total surface areas of microstructural surfaces per unit volume, and integral mean curvature of surfaces in a 3D microstructure can be estimated via unbiased sampling of the 3D microstructure using planes or surfaces as sampling probes [23–28]. Consider estimation of total surface area S_1 of surfaces of interest in the 3D microstructure of a specimen of volume Σ. Suppose this 3D microstructure is sampled in an unbiased[3] manner with another set of probe surfaces. This can be done by placing the probe surfaces of uniform random orientations at a large number of uniform random locations in the microstructural space of interest. Let S_{probe} be the total area of the probe surfaces. The intersections of the probe surfaces with the microstructural surfaces of interest create lines of intersection. Let L_{total} be the total length of these lines. Stochastic geometry gives the following general relationship [23–28,39].

$$\frac{S_1}{\Sigma} = \frac{4}{\pi}\frac{L_{total}}{S_{probe}} \tag{8}$$

[3] Unbiased sampling implies that sampling at all locations with probes having all possible orientations is equally likely. Therefore, each microstructural feature has the same probability of being included in the statistical sample.

or,

$$\frac{S_1}{\Sigma} = \frac{4}{\pi}\frac{L_{total}/\Sigma}{S_{probe}/\Sigma} \tag{9}$$

Eqs. (8) and (9) are applicable to any 3D microstructure and the probe surfaces of any geometry (for example, probes can be surfaces of ellipsoids, polyhedrons, or planes). The only requirement is that the sampling must be unbiased, which implies that the surfaces of the probes and the surfaces of interest must have uniform random orientations and locations with respect to one another. This requirement is satisfied in our extended microstructure having uniform random orientations and locations of YSZ and LSM particles. Now, consider estimation of the total length of the TPB per unit volume $(L_{TPB})_{ex}$ in the extended microstructure using Eq. (9). Consider a thought experiment where the total surface area of YSZ particle surfaces per unit volume $(S_{YZ})_{ex}$ is to be estimated (i.e., S_1/Σ in Eq. (9)) using LSM particle surfaces as *probes* via application of Eq. (9). Let $(S_{LM})_{ex}$ be the total area of the LSM surfaces per unit volume (i.e., probe surface area per unit volume, S_{probe}/Σ). Intersections of YSZ and probe LSM surfaces are the TPB whose total length per unit volume is $(L_{TPB})_{ex}$ (i.e., L_{total}/Σ). For isotropic uniform random YSZ and LSM particles, Eq. (9) gives the following result[4].

$$(S_{YZ})_{ex} = \frac{4}{\pi}\left[\frac{(L_{TPB})_{ex}}{(S_{LM})_{ex}}\right] \tag{10}$$

or,

$$(L_{TPB})_{ex} = \frac{\pi}{4}(S_{YZ})_{ex}(S_{LM})_{ex} \tag{11}$$

Combining Eqs. (7) and (11) gives the following expression for the triple phase boundary length per unit volume L_{TPB} in the corresponding real microstructure.

$$L_{TPB} = \frac{\pi}{4}\theta_P(S_{YZ})_{ex}(S_{LM})_{ex} \tag{12}$$

Let $\langle S_Y\rangle$ and $\langle S_L\rangle$ be the mean values of the surface areas and let $\langle V_Y\rangle$ and $\langle V_L\rangle$ be the mean volumes of the YSZ and LSM particles, respectively. Let N_Y and N_L be the number of YSZ and LSM particles per unit volume, respectively. Therefore,

$$(S_{YZ})_{ex} = \langle S_Y\rangle N_Y \tag{13}$$

$$(S_{LM})_{ex} = \langle S_L\rangle N_L \tag{14}$$

$$(\theta_Y)_{ex} = \langle V_Y\rangle N_Y \tag{15}$$

$$(\theta_L)_{ex} = \langle V_L\rangle N_L \tag{16}$$

Combining Eqs. (5) and (13)–(16) yields the following result.

$$(S_{YZ})_{ex}(S_{LM})_{ex} = \frac{\langle S_Y\rangle\langle S_L\rangle}{\langle V_Y\rangle\langle V_L\rangle}\frac{\alpha}{(1+\alpha)^2}[\ln(\theta_P)]^2 \tag{17}$$

Combining Eqs. (12) and (17) gives the following result for (L_{TPB}).

$$L_{TPB} = \frac{\pi}{4}\frac{\alpha}{(1+\alpha)^2}\left\{\theta_P[\ln(\theta_P)]^2\right\}\left[\frac{\langle S_Y\rangle\langle S_L\rangle}{\langle V_Y\rangle\langle V_L\rangle}\right] \tag{18}$$

Eq. (18) is applicable to YSZ and LSM particles of any convex shapes and any size-shape distributions, provided that the angular orientations and locations of the YSZ and LSM particles are uniform random. The YSZ and LSM particles need not be of the same convex morphology or have the same size-shape distribution; the only

[4] If the sampling surfaces are planes, Eq. (10) reduces to the following stereological relationship [23–28,39], which is used to estimate the total microstructural surfaces of interest per unit volume S_1/Σ from the measurements of the total length of the boundary traces in the random 2D sections per unit area L_A [23–25,39].

$$\frac{S_1}{\Sigma} = \frac{4}{\pi}L_A.$$

requirement is that each particle must be convex. For example, YSZ particles can be spheres and LSM particles can be plate shaped. The result is valid for any porosity volume fraction θ_P, and for any value of the ratio of the amounts of YSZ and LSM, α. It is convenient to write Eq. (18) in the following form.

$$L_{TPB} = \frac{\pi}{4} F_1(\alpha) F_2(\theta_P) \left[\frac{\langle S_Y \rangle \langle S_L \rangle}{\langle V_Y \rangle \langle V_L \rangle} \right] \tag{19}$$

where

$$F_1(\alpha) = \frac{\alpha}{(1+\alpha)^2} \tag{20}$$

and,

$$F_2(\theta_P) = \theta_P \left[\ln(\theta_P) \right]^2 \tag{21}$$

In Eq. (19), the term $F_2(\theta_P)$ *explicitly* brings out the dependence of L_{TPB} on the porosity volume fraction θ_P, whereas the term $F_1(\alpha)$ captures the dependence of L_{TPB} on the relative proportions of YSZ and LSM, α, *explicitly*. Recall that α is equal to θ_Y/θ_L (see Eq. (3)). Therefore, the factors $F_1(\alpha)$ and $F_2(\theta_P)$ completely determine how L_{TPB} varies with the volume fractions of the three phases, YSZ, LSM, and porosity. The dependence of L_{TPB} on the morphology, the mean sizes, and size-shape distributions of the YSZ and LSM particles is contained in the last term in the square bracket in Eq. (20), i.e., $\langle S_Y \rangle \langle S_L \rangle / \langle V_Y \rangle \langle V_L \rangle$. The mean volumes and surface areas of YSZ and LSM particles can be expressed as follows.

$$\langle S_Y \rangle = K_{1Y} \langle D_Y^2 \rangle \tag{22}$$

$$\langle S_L \rangle = K_{1L} \langle D_L^2 \rangle \tag{23}$$

$$\langle V_Y \rangle = K_{2Y} \langle D_Y^3 \rangle \tag{24}$$

$$\langle V_L \rangle = K_{2L} \langle D_L^3 \rangle \tag{25}$$

In the above equations, K_{1Y}, K_{1L}, K_{2Y}, K_{2L} are the shape factors that depend on the shape(s) of the YSZ and LSM particles. $\langle D_Y^2 \rangle$ is the mean value of the *square* of the YSZ particle sizes (i.e., the second moment of the size distribution), and $\langle D_L^2 \rangle$ is the mean value of *square* of the LSM particle sizes[5]. Similarly, $\langle D_Y^3 \rangle$ is the mean value of the *cube* of the YSZ particle sizes (i.e., the third moment of the size distribution), and $\langle D_L^3 \rangle$ is the mean value of *cube* of the LSM particle sizes. Combining Eq. (19) with the Eqs. (22)–(25) gives the following result.

$$L_{TPB} = \frac{\pi}{4} F_1(\alpha) F_2(\theta_P) F_3(K) \frac{\langle D_Y^2 \rangle \langle D_L^2 \rangle}{\langle D_Y^3 \rangle \langle D_Y^3 \rangle} \tag{26}$$

where

$$F_3(K) = \frac{K_{1Y} K_{1L}}{K_{2Y} K_{2L}} \tag{27}$$

$F_3(K)$ depends only on the shapes of the YSZ and LSM particles. For spherical YSZ and LSM particles, $F_3(K)$ is equal to 36 and the diameters are the size parameters. It remains to deconvolute the effects of the mean particle sizes, spreads, and skewness of the size distributions of YSZ and LSM on the L_{TPB} that are contained in the term $\langle D_Y^2 \rangle \langle D_L^2 \rangle / \langle D_Y^3 \rangle \langle D_L^3 \rangle$ in Eq. (26). Let D represent the particle sizes in a size distribution. The arithmetic mean particle size $\langle D \rangle$, the variance σ^2, the coefficient of variation CV, and the skewness γ of a size distribution function $f(D)$ are defined as follows [40,41].

$$\langle D \rangle = \int D f(D) dD \tag{28}$$

$$\sigma^2 = \int \left[D - \langle D \rangle \right]^2 f(D) dD = \langle D^2 \rangle - \langle D \rangle^2 \tag{29}$$

$$\mathrm{CV} = \frac{\sigma}{\langle D \rangle} \tag{30}$$

$$\gamma = \frac{1}{\sigma^3} \int \left[D - \langle D \rangle \right]^3 f(D) dD \tag{31}$$

Combining Eqs. (29)–(31) gives the following results.

$$\langle D^2 \rangle = \langle D \rangle^2 (1 + \mathrm{CV}^2) \tag{32}$$

$$\langle D^3 \rangle = \langle D \rangle^3 (1 + 3\mathrm{CV}^2 + \gamma \mathrm{CV}^3) \tag{33}$$

Substituting Eqs. (32) and (33) into Eq. (26) leads to the following result.

$$L_{TPB} = \frac{\pi}{4} F_1(\alpha) F_2(\theta_P) F_3(K) F_4(\mathrm{CV}, \gamma) \frac{1}{\langle D_Y \rangle \langle D_L \rangle} \tag{34}$$

where

$$F_4(\mathrm{CV}, \gamma) = \frac{(1 + \mathrm{CV}_Y^2)(1 + \mathrm{CV}_L^2)}{(1 + 3\mathrm{CV}_Y^2 + \gamma_Y \mathrm{CV}_Y^3)(1 + 3\mathrm{CV}_L^2 + \gamma_L \mathrm{CV}_L^3)} \tag{35}$$

In Eq. (34), CV_Y and CV_L are coefficient of variation, and γ_Y and γ_L are skewness parameters of the YSZ and LSM powder size distributions, respectively. Note that $F_4(\mathrm{CV},\gamma)$ depends *only* on the coefficient of variation and the skewness of the size distributions, and it *explicitly* brings out the effect of these parameters on L_{TPB}.

Eq. (34) predicts that for given volume fractions of YSZ, LSM, and porosity, and the coefficient of variation and the skewness of the YSZ and LSM size distributions, and particle morphologies, L_{TPB} is inversely proportional to the mean size of YSZ particles, $\langle D_Y \rangle$, and the mean size of LSM particles, $\langle D_L \rangle$. Therefore, the finer the mean particle sizes of YSZ and/or LSM, the higher is the total length of the TPB per unit volume, L_{TPB}. Similar trend has been predicted by earlier simulations and analytical models for L_{TPB} in composite cathodes [15,17,42]. Nonetheless, earlier analytical treatments of L_{TPB} were based on an assumption that all YSZ and LSM particles are of the same size, and therefore, did not capture the separate effects of different YSZ and LSM mean sizes on the L_{TPB}. The present result shows that the L_{TPB} can be increased either by decreasing the mean size of YSZ particles, or LSM particles, or by decreasing the mean sizes of both the particle populations, and it *explicitly* captures the dependence of L_{TPB} on the mean particle sizes. Eq. (34) also explicitly brings out the effects of other geometric characteristics on L_{TPB} through the functions $F_1(\alpha)$, $F_2(\theta_P)$, $F_3(K)$, and $F_4(\mathrm{CV},\gamma)$, which facilitates the parametric studies. Analysis of the results, comparison with experimental data, and parametric studies for microstructural engineering to optimize L_{TPB} are presented in the next section.

3. Results and discussion

A stochastic geometry based approach is presented for geometric modeling of total triple phase boundary length per unit volume L_{TPB} in the microstructure of composite SOFC cathodes. The model is based on the assumptions that the YSZ and LSM particles are convex, they have uniform random angular orientations and spatial locations, and there are no spatial correlations in their locations. The model permits the particles to freely overlap and intersect in the extended microstructure. The approach enables tractable analytical treatment of the geometric problem, and leads to closed form analytical solution that relates L_{TPB} to numerous geometric parameters including volume fractions of the phases; morphologies/shapes of particles; and the mean sizes, the coefficient of variation, and the skewness of YSZ and LSM size distributions. Although Eq. (34) is derived in the context of the microstructures of SOFC composite cathodes, it is equally applicable to the microstructures of SOFC

[5] In general, the mean of the square of the particles sizes is not equal to the square of the mean value of the particle sizes, except when all particles are of the same size. Similarly, the mean of the cube of the particles sizes is not equal to the cube of the mean value of the particle sizes, except when all particles are of the same size.

anodes, or to any three phase uniform random isotropic microstructure. Unlike the earlier analytical models [17,42], to calculate the L_{TPB} using Eq. (34), it is not necessary to know the mean coordination number of the particles, which is difficult to measure experimentally (because reconstruction of 3D microstructure is required [22]), and is difficult to compute from theoretical considerations without making numerous simplifying assumptions. Further, earlier models and simulations assumed that YSZ and LSM particles are mono-sized spheres, and therefore, did not reveal the effects of the morphology/shape of the YSZ and LSM particles and the powder characteristics such as the coefficient of variation (a measure of spread in the particle sizes) and the skewness of the size distributions on L_{TPB}.

Eq. (34) is developed for prediction of L_{TPB} in powder-processed composite cathodes fabricated via sintering of a *powder mix* containing YSZ and LSM powder particles. It may have to be modified for the composite cathodes fabricated using other processing routes. It is important to point out that the present model predicts the *total* (active plus inactive) triple phase boundary length. Some TPB are *not* topologically connected to the electrical conducting paths and gas permeating pores in the microstructure, and therefore, do not participate in the electrochemical processes. In a subsequent contribution it will be shown that *beyond the percolation thresholds*, about 90% of the total triple phase boundary length is connected to the electrical conducting paths and gas permeating pores in the microstructure [51].

All TPB that are connected to the electrical conductive paths and gas permeating pores also may not be *electrochemically active*. The electrochemical activity at the TPB depend on the availability of the electro-active species involved in the electrochemical reactions (e.g., $V_O^{\bullet\bullet}$, $h^{\bullet}$, and O_2) at or near the TPB, which is dictated by $V^{\bullet\bullet}$ transport through YSZ, $h^{\bullet\bullet}$ transport through LSM, and O_2 transport through the pores of the electrode. For a typical YSZ/LSM cathode with sufficient porosity for O_2 transport, the electrochemical activity induced by a triple phase boundary often diminishes with the distance from the interface between the YSZ/LSM composite cathode and the YSZ electrolyte because the ionic conductivity of YSZ is orders of magnitudes smaller than the electronic conductivity of LSM. Therefore, only the triple phase boundary segments within a certain *effective* membrane thickness (which is less than the geometric thickness of the composite cathode) that are connected to the electrical conductive paths and gas permeating pores are electrochemically active [17,50]. Nonetheless, it can be said that in a composite cathode having isotropic uniform random microstructure, an increase in the L_{TPB} is expected to lead to an increase in the electrochemically active triple phase boundary length per unit volume. Therefore, the microstructural engineering to optimize the L_{TPB} using the present approach should also lead to an increase in the electrochemically active triple phase boundary length per unit volume, which is likely to improve the performance of the cathode.

The present model is applicable only to the microstructural volume segments that are at least of the size of the smallest statistical representative volume element[6] (RVE) of the corresponding infinite global microstructure. This is true of *any* theoretical model or simulation. Therefore, the present results may not be applicable to very thin composite cathode membranes (i.e., thickness on the order of the particle size). In a subsequent contribution, we will examine at what ratio of membrane thickness to mean particle size the microstructural segment becomes sufficiently large to be treated as RVE.

[6] A representative volume element of a microstructure is such that if different volume elements of that size are chosen at random anywhere in the corresponding infinite microstructure all of them will have the same properties.

The input size distribution data (mean sizes, coefficient of variation, and skewness) needed for the present model pertain to the YSZ and LSM particles present in the powder mix *after ball milling* (or after any attrition process used to obtain a homogeneous powder mix) and prior to sintering (i.e., not size distributions in the unmixed initial powders of YSZ and LSM) because operations like ball milling fragment the particles and alter the size distributions. Further, if the powder particles agglomerate during any of the powder processing steps then the distribution characteristics of the agglomerated powders must be used in Eq. (34).

The present approach is purely geometric: it does not incorporate the *physics* of the sintering process. Therefore, in its present form, the model does not account for coarsening of the microstructure during sintering that can decrease the L_{TPB}. In the case of LSM/YSZ composite cathodes, the sintering is typically carried out at temperatures below 1200 °C to minimize such coarsening so that the fine microstructure (and higher L_{TPB}) can be retained after sintering [11,12], and in such cases, Eq. (34) can predict the L_{TPB} in a precise manner.

It is important to point out that the earlier modeling and simulation efforts were also either geometric or involved substantial simplifying assumptions concerning the microstructural geometry and the physics of the sintering process. This is because a geometrically general and rigorous sintering physics based modeling of L_{TPB} is too complex to be analytically tractable or computationally feasible. Consequently, it is of interest to compare the predictions of the present model with the experimental data on L_{TPB} and earlier models and simulations.

3.1. Comparison with experimental data

To verify the present model (Eq. (34)), the following experimental data are needed: (i) experimentally estimated L_{TPB} either via reconstruction of 3D microstructure or by using the stereological techniques, (ii) volume fractions of YSZ, LSM, and porosity, and (iii) mean sizes, coefficient of variation, and skewness of the YSZ and LSM particle size distributions after ball milling or powder mixing operations and prior to sintering. There have been only two experimental measurements of L_{TPB} in composite SOFC cathode microstructures reported in the literature [47,49], and one study has reported L_{TPB} data in SOFC anode microstructure [48]. In all of these cases, the particle size distribution data needed to verify Eq. (34) have not been reported. Nonetheless, Eq. (12) (from which Eq. (34) has been obtained without any additional assumptions) can be cast into a form that can be verified using the available data. For an isotropic uniform random microstructure, it can be shown that [43,44]:

$$S_{YP} = \theta_P (S_Y)_{ex} \tag{36}$$

and,

$$S_{LP} = \theta_P (S_L)_{ex} \tag{37}$$

S_{YP} and S_{LP} are the total surface areas of YSZ/porosity surfaces and LSM/porosity surfaces per unit volume of specimen in the real microstructure, which can be experimentally measured. Therefore, combining Eqs. (12), (36) and (37) leads to the following result.

$$L_{TPB} = \frac{\pi}{4} \frac{S_{YP} S_{LP}}{\theta_P} \tag{38}$$

An equation analogous to Eq. (38) was reported earlier in the context of microstrucutral evolution during phase transformations [45]. It is important to point out that Eq. (38) is applicable to any isotropic uniform-random microstructure: its applicability is not limited to the microstructures of powder processed composite cathodes. Nonetheless, the use of Eq. (38) requires the experimental microstrucutral data, and therefore, unlike Eq. (34), it cannot

predict L_{TPB} in an a priori manner from initial raw material characteristics (for example, size distributions of initial powder particles) before fabrication of the composite cathode. Wilson et al. [46] reconstructed 3D microstructure of SOFC *anode* containing YSZ, Ni, and porosity, and measured L_{TPB}, porosity volume fraction θ_P, and total surface areas of YSZ-porosity, S_{YP}, and Ni-Porosity, S_{NP} per unit volume. As the anode contains Ni instead of LSM, in Eq. (38), S_{LP} has to be replaced by S_{NP}. Wilson et al. reported L_{TPB} equal to 4.28 $\mu m\,\mu m^{-3}$, and θ_P, S_{YP}, and S_{NP} equal to 0.195, 0.5 and 1.9 $\mu m^2\,\mu m^{-3}$, respectively. Substituting these data in Eq. (38) yields the value of L_{TPB} equal to 3.83 $\mu m\,\mu m^{-3}$, which is in good agreement with the experimental value of 4.28 $\mu m\,\mu m^{-3}$.

Zhang et al. [49] estimated the L_{TPB} using atomic force microscopy and stereological techniques in a composite LSM/YSZ cathode[7] to be equal to $10.8 \pm 1.15\ \mu m\,\mu m^{-3}$. The experimentally measured volume fractions of YSZ and LSM were (0.28 ± 0.027) and (0.26 ± 0.018), respectively, and the experimentally measured S_{YP} and S_{LP} were (3.87 ± 0.21) and $(2.32 \pm 0.3)\ \mu m^2\,\mu m^{-3}$, respectively. Recall that θ_P is equal to $(1 - \theta_Y - \theta_L)$. Substituting these data into Eq. (38) yields the computed value of L_{TPB} equal to $(15.8 \pm 4.3)\mu m\,\mu m^{-3}$. The large error bar in the computed L_{TPB} is because each of the three experimentally measured parameters on the right hand side in Eq. (38) has a statistical sampling error. Considering large sampling error associated with computed L_{TPB}, there is reasonable agreement between the computed and experimentally measured L_{TPB} values.

Wilson et al. [47] performed 3D microstructure reconstructions of a series of composite cathodes having different proportions of YSZ and LSM, and reported that the L_{TPB} is in the range of 8–10 $\mu m\,\mu m^{-3}$ and it is not sensitive to the proportion of YSZ and LSM. This trend can be predicted from Eq. (34), where the dependence of L_{TPB} on the relative proportion of YSZ and LSM represented by parameter α resides in the function $F_1(\alpha)$. When α is in the range 0.5–2.5, $F_1(\alpha)$ is in the range of (0.225 ± 0.0225), i.e., a variation of ±10%. Thus, L_{TPB} is not sensitive to relative proportion of YSZ and LSM when α is in the range 0.5–2.5 (the range for practical applications), as observed by Wilson et al. [47].

3.2. Comparison with simulations and models reported in literature

Ali et al. [15] performed simulations of composite cathode microstructures involving random packing of impenetrable mono-sized spheres followed by 10% dilation of the particle diameters to create the TPB. The simulations predict that the L_{TPB} decreases with increasing particle size, with a trend similar to that predicted by Eq. (34). Nonetheless, the simulated triple phase boundary length reported by these researchers is the *active* L_{TPB}, whereas Eq. (34) predicts the total (active plus inactive) L_{TPB}. As mentioned earlier, beyond the percolation threshold, about 90% or more of the total L_{TPB} is active L_{TPB} [51], and therefore, there is no significant difference between the two. Consequently, the simulated L_{TPB} reported by Ali et al. [15] can be compared with the predictions of Eq. (34) for the porosity volume fractions in the range of 0.3–0.5, and relative proportions of YSZ and LSM (i.e., parameter α in Eq. (34)) in the range of 0.5–2.5. Ali et al. [15] assumed that the YSZ and LSM particles are mono-sized spheres. For these particle characteristics, in Eq. (34), $F_3(K) = 36$ and $F_4(CV,\gamma) = 1$. The L_{TPB} computed from Eq. (34) using these values of $F_3(K)$ and $F_4(CV,\gamma)$ for the porosity volume fractions of 0.3 and α in the range of 0.5–1.5 are given in Table 1 for comparison with the simulated L_{TPB} values obtained by Ali et al. [15]. There is a good agreement between the values of simulated L_{TPB} obtained by Ali et al. [15] and the corresponding values computed using Eq. (34).

Schneider et al. [17] have proposed the following analytical equation for total (active plus inactive) L_{TPB} based on random packing of mono-size spheres of radius r.

$$L_{TPB} = \frac{3d}{r^2}\sqrt{1 - \left(\frac{d_0}{d}\right)^{1/3}}\,\phi_{io}(1 - \phi_{io})Z \tag{39}$$

where,

$$\phi_{io} = \frac{\theta_Y}{\theta_Y + \theta_L} = \frac{\alpha}{1 + \alpha} \tag{40}$$

In Eq. (39), d_o is the density of the powder mix before sintering, d is the density after sintering, and Z is the mean coordination number of the particles. Interestingly, the $\phi_{io}(1 - \phi_{io})$ factor in Eq. (39) is equal to $\alpha/(1 + \alpha)^2$, i.e., $F_1(\alpha)$ in Eq. (34), and for mono-sized YSZ and LSM having the same radius r, Eqs. (39) and (34) predict that L_{TPB} is inversely proportional to the square of the particle size. However, Eq. (34) is applicable to YSZ and LSM particles having any size distribution and convex particle shape(s). On the other hand, Schneider et al. assume that YSZ and LSM particles are spherical and mono-sized, and to compute L_{TPB} using their equation it is necessary to *assume* a value for the mean coordination number Z and the density of initial powder mix d_o. Further, Eq. (39) leads to a physically unacceptable limit as d approaches 1 (i.e., fully dense material). In the limit of $d \to 1$ (i.e., porosity volume fraction $\theta_P \to 0$) the L_{TPB} must approach zero because YSZ-LSM-porosity TPB cannot exist when there are no pores. However, Eq. (39) predicts a non-zero value of L_{TPB} as $d \to 1$, which is physically untenable. On the other hand, the L_{TPB} predicted by Eq. (34) reaches the correct limit of zero as the volume fraction of porosity θ_P approaches zero or one. Schneider et al. computed the values of L_{TPB} from Eq. (39) assuming $d_0 = 0.5$ and $Z = 6.3$. For these values of d_0 and Z, Eq. (39) gives L_{TPB} in the range of 1.1–1.2 $\mu m\,\mu m^{-3}$ when $r = 1\ \mu m$ and $D = 0.75$ for ϕ_{io} in the range of 0.3–0.7. For the same range of ϕ_{io}, and r and d values, Eq. (34) yields L_{TPB} in the range of 0.7–0.84 $\mu m\,\mu m^{-3}$, which is somewhat lower than that obtained from Eq. (39). These differences are probably due to the values of d_0 and Z assumed by Schneider et al. (somewhat different values of these parameters lead to better agreement) and/or because Eq. (39) is inaccurate at high values of d, as it gives physically unacceptable nonzero value of L_{TPB} as d approaches one.

3.3. Parametric studies

Eq. (34) predicts that for given morphologies, volume fractions, coefficient of variation, and skewness of the YSZ and LSM particle populations, the L_{TPB} is inversely proportional to the mean sizes of YSZ and LSM particles, $\langle D_Y \rangle$ and $\langle D_L \rangle$. This trend is also predicted by earlier simulations and analytical models [15,17,42]. Nonetheless, earlier analytical treatments of L_{TPB} assumed that YSZ and LSM particles are spherical and of the same mono-size, and therefore, did not reveal the separate effects of different YSZ and LSM mean sizes on the L_{TPB}. The present result shows that L_{TPB} can be increased by decreasing the mean size of YSZ or LSM particles, or of both YSZ and LSM particles, and it *explicitly* captures the dependence of L_{TPB} on the mean particle sizes.

3.3.1. Effect of relative proportion of YSZ and LSM on L_{TPB}

The relative proportion of YSZ and LSM is specified by the parameter α, which is equal to the ratio of the volume fraction of YSZ and LSM, $[\theta_Y/\theta_L]$. In Eq. (34), the dependence of L_{TPB} on α is expressed by the function $F_1(\alpha)$. In principle, α can vary from zero to infinity, and at these two limits, $F_1(\alpha)$ and L_{TPB}, approach zero as they must for the model to be physically tenable. Nonetheless, for SOFC applications, YSZ, LSM, and porosity phases must topologically percolate. Therefore, each phase should have volume fraction in the

[7] The error bars are statistical sampling errors for 95% confidence interval.

Table 1
Comparison of the TPB length reported in Ali et al.[15] and calculated with Eq. (34).

θ_Y	α	θ_P	D_Y, D_L	Simulated L_{TPB} ($\mu m\,\mu m^{-3}$) (Ali et al. [15])	Computed L_{TPB} ($\mu m\,\mu m^{-3}$) Eq. (34)
22–28%	0.46–0.67	30%	1 μm, 2 μm	1.2–1.3	1.3–1.5
37–42%	1.1–1.5	30%	2 μm, 1 μm	1.2–1.3	1.3–1.5
28–42%	0.7–1.5	30%	2 μm, 2 μm	0.5–0.6	0.7–0.8

range 0.25–0.5 such that the sum of the three volume fractions is equal to one. With these constraints on the volume fractions, the parameter α is constrained in the range 0.5–2.5. Fig. 1 shows the variation of $F_1(\alpha)$ with α. Observe that $F_1(\alpha)$ reaches the maximum value of 0.25 when α is equal to 1, and it varies only from 0.225 to 0.25 as α varies from 0.5 to 2.5. Consequently, L_{TPB} does not vary by more than 10% in the range of α values of interest in SOFC composite cathode applications where all three phases must topologically percolate.

3.3.2. Effect of porosity volume fraction on L_{TPB}

In Eq. (34), the dependence of L_{TPB} on the porosity volume fraction θ_P is captured in the function $F_2(\theta_P)$, which is equal to $\{\theta_P[\ln\theta_P]^2\}$. In principle, θ_P can vary from zero to one. At these two limits, $F_2(\theta_P)$ and consequently L_{TPB}, approach zero as they must for the model to be physically tenable. Fig. 2 shows the variation of $F_2(\theta_P)$ with θ_P. Note that $F_2(\theta_P)$ has a maximum value of 0.541, when θ_P is equal to 0.135. Nonetheless, for practical SOFC composite cathode applications, YSZ, LSM, and porosity phases, must percolate. Therefore, θ_P is expected to be in the range of 0.2–0.5. As θ_P increases from 0.2 to 0.5, $F_2(\theta_P)$ decreases from 0.52 to 0.24 (i.e., by a factor of about two). Thus, for SOFC composite cathode applications, for given values of α, and mean particle sizes, CV, and the skewness of the YSZ and LSM powder populations, the highest value of L_{TPB} is obtained at the *lowest* porosity volume fraction that permits sufficient percolation and connectivity of pores for gas permeability.

3.3.3. Effects of CV and skewness on L_{TPB}

In Eq. (34), for given mean sizes of YSZ and LSM powder particles, the dependence of L_{TPB} on the coefficient of variation CV and the skewness of YSZ and LSM particle size distributions is contained in the function $F_4(\mathrm{CV},\gamma)$, given by Eq. (35). For mono-sized YSZ and LSM, coefficients of variation, $\mathrm{CV_Y}$ and $\mathrm{CV_L}$, and skewness, γ_Y and γ_L are zero, and therefore, $F_4(\mathrm{CV},\gamma)$ is equal to one. It is well known that for any physically realizable size distribution function, skewness $\gamma \geq (-2/\mathrm{CV})$, and therefore, $F_4(\mathrm{CV},\gamma) \leq 1$. Consequently, for given relative proportion of YSZ and LSM, porosity volume fraction, and mean particle sizes of YSZ and LSM, the L_{TPB} has the maximum value for *mono-size* powders of YSZ and LSM. Any spread in the size distribution (i.e., non-zero CV) decreases L_{TPB}. For symmetric size distribution functions such as the normal distribution, the skewness γ is equal to zero. For such populations, as $\mathrm{CV_Y}$ and $\mathrm{CV_L}$ become very large (strictly speaking, as they go to infinity), $F_4(\mathrm{CV},\gamma)$ approaches 1/9. Therefore, L_{TPB} can decrease almost by an order of magnitude as coefficients of variation of YSZ and LSM powder populations increase from zero (corresponding to mono-size) to infinity. Thus, there is a strong dependence of $F_4(\mathrm{CV},\gamma)$ on CV. For example, relatively small values $\mathrm{CV_Y} = \mathrm{CV_L} = 0.5$ in normal distributions of YSZ and LSM powders reduce F_4 (CV,γ) to 0.51 from the value of 1.0 for mono-size powders (i.e., $\mathrm{CV_Y} = \mathrm{CV_L} = 0$), which leads to a decrease in L_{TPB} approximately by a factor of 2 as compared to that for the mono-sized powders. Therefore, mono-size particle populations (although YSZ and LSM can have different mono-sizes) optimize L_{TPB} for given mean sizes, shapes, and volume fractions of YSZ and LSM.

Skewness of a size distribution (see Eq. (31)) can be negative, positive, or zero. Inspection of Eq. (35) reveals that for given values of CV of YSZ and LSM particles, $F_4(\mathrm{CV},\gamma)$ is higher (and therefore, L_{TPB} is higher) for YSZ and LSM populations that have a *negative skewness*, than for the size distributions that have *positive* skewness. In a distribution having negative skewness, the mean is lower than the median (which is lower than the mode). Therefore, negative skewness leads to a long left tail in a size distribution. As particle sizes cannot be negative, clearly there is a limit on the extent to which the skewness can be negative in a physically realizable size distribution function. It is not clear if the current powder processing technologies can yield YSZ and LSM powder populations with a specified CV and/or skewness values, but if that is possible, Eqs. (34) and (35) provide a framework to compute how much improvement in the L_{TPB} is possible via such process designs.

3.3.4. Effects of powder particle shape/morphology on L_{TPB}

Earlier investigations on modeling and simulations of L_{TPB} assumed that YSZ and LSM particles are spherical, and therefore, did not reveal the effects of particle shape(s) on L_{TPB}. In Eq. (34), the effect of particle shape(s) on L_{TPB} is contained in the function $F_3(K)$, defined in Eq. (27). For spherical YSZ and LSM particles, $F_3(K)$ is equal to 36. For given size distributions and the volume fractions of YSZ and LSM, an increase in the function $F_3(K)$ leads to an

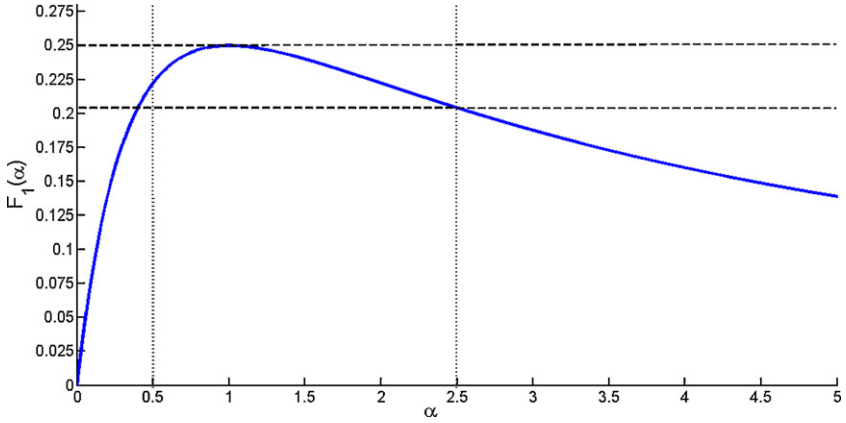

Fig. 1. Plot of $F(\alpha)$ versus α.

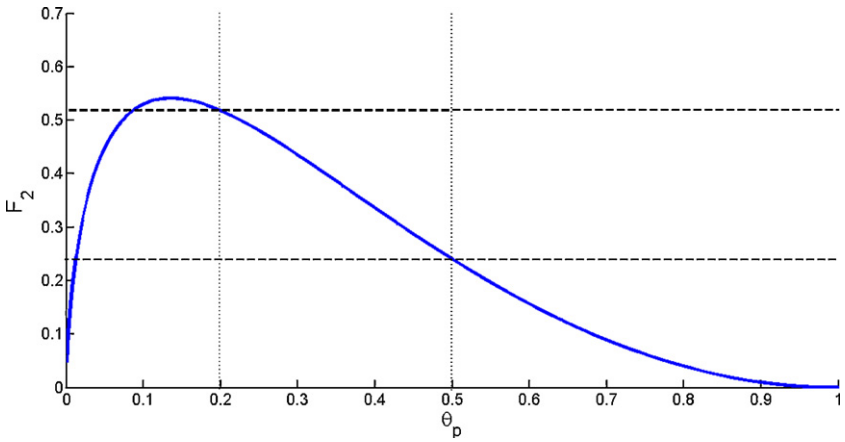

Fig. 2. Plot of $F_2(\theta_P)$ versus θ_P.

increase in L_{TPB}. Therefore, it is of interest to determine if there are particle shape(s) that increase the value of $F_3(K)$ substantially above 36. For such an analysis it is imperative to use the same geometric measure of "size" for particles of different shapes, because the objective is to determine which shape(s) increase the L_{TPB} for constant values of mean sizes, size distributions, and volume fractions of the phases. For convex particles, the orientation averaged particle caliper diameter[8] is a rigorously defined unique measure of "size" that can be used to compare the "sizes" of convex particles of different shapes (say, plates and spheres). For a spherical particle, the caliper diameter is the same in all orientations, and therefore, the orientation averaged caliper diameter of a sphere is equal to its diameter. The orientation averaged caliper diameter D of any convex particle can be computed by using Minkowski's equation of integral geometry given below [24].

$$D = \frac{1}{2\pi}\left[\iint H dA + \frac{1}{2}\int \chi d\lambda\right] \tag{41}$$

In Eq. (41) H is the local mean curvature of an infinitesimal surface element dA on the smooth surface(s) of the convex particle and the surface integral is to be performed over all smooth surfaces of the particle. The second term arises from the edges (if present) on the particle surface(s) and χ is the dihedral angle of an edge element of length $d\lambda$. The second integral is to be performed over all the edges of the particle. If the particle has only smooth surfaces (for example, ellipsoids), then the second integral is zero. In the particle population having a distribution of D values, the mean size is denoted by $\langle D\rangle$. In Eq. (34), $\langle D_Y\rangle$ and $\langle D_L\rangle$ are these measures of the mean sizes of the YSZ and LSM particles.

For parametric analysis it is convenient to use cylinder as a model shape to generate equiaxed, plate-like (or flake-like), and needle-like morphologies by varying the ratio of the cylinder radius R and length L. The volume V_{cyl}, surface area S_{cyl} of a cylinder are given as follows.

$$V_{cyl} = \left[\pi\left(\frac{L}{R}\right)\right]R^3 \tag{42}$$

$$S_{cyl} = 2\pi\left[1+\left(\frac{L}{R}\right)\right]R^2 \tag{43}$$

[8] Caliper diameter is equal to the distance between two parallel tangent planes of a particle. For a convex particle, there are two (and exactly two) parallel tangent planes for every angular orientation. Therefore, there is a unique caliper diameter for each orientation. Caliper diameter can vary with the tangent plane orientation. The orientation averaged caliper diameter D is obtained by averaging the caliper diameter over all tangent plane orientations.

Applying Eq. (41) to surfaces and edges of a cylinder yields the following result for the orientation averaged caliper diameter D of a cylinder.

$$D = \frac{1}{2}\left[\pi + \left(\frac{L}{R}\right)\right]R \tag{44}$$

Combining Eqs. (42)–(44) yields the following result.

$$V_{cyl} = \frac{8\pi(L/R)}{[\pi+(L/R)]^3}D^3 \tag{45}$$

and,

$$S_{cyl} = \frac{8\pi[1+(L/R)]}{[\pi+(L/R)]^2}D^2 \tag{46}$$

For cylindrical YSZ and LSM particles having constant (R/L) ratio, one can write:

$$\langle V_Y\rangle = \frac{8\pi(L/R)}{[\pi+(L/R)]^3}\langle D_Y^3\rangle \tag{47}$$

$$\langle S_Y\rangle = \frac{8\pi[1+(L/R)]}{[\pi+(L/R)]^2}\langle D_Y^2\rangle \tag{48}$$

$$\langle V_L\rangle = \frac{8\pi(L/R)}{[\pi+(L/R)]^3}\langle D_L^3\rangle \tag{49}$$

$$\langle S_L\rangle = \frac{8\pi[1+(L/R)]}{[\pi+(L/R)]^2}\langle D_L^2\rangle \tag{50}$$

$\langle D_Y^3\rangle$, $\langle D_L^3\rangle$, $\langle D_L^2\rangle$, $\langle D_Y^2\rangle$ are the population average values of D^3 and D^2 for YSZ and LSM size distributions, respectively. Comparing Eqs. (47)–(50) with Eqs. (22)–(25) yields the shape factors K_{1Y}, K_{1L}, K_{2Y}, K_{2L}. Substituting these shape factors in Eq. (27) gives the following result for cylindrical particle populations of YSZ and LSM having constant (R/L).

$$F_3(K) = [1+(L/R)]^2[1+\pi(R/L)]^2 \tag{51}$$

Fig. 3 shows a plot of $F_3(K)$ versus (R/L). Observe that (i) for any value of (R/L), $F_3(K)$ for cylindrical particles is higher than that for spherical particles, (ii) $F_3(K)$ reaches high values for large (R/L) ratios that correspond to plate-like or flake-like particle shapes, and (iii) $F_3(K)$ reaches high values also when (R/L) approaches zero, which corresponds to needle-like shapes. Even for equiaxed cylindrical particles ($(R/L)=0.5$), $F_3(K)=59.44$, which is higher than the value of 36 for the spherical particles. For (R/L) equal to 2, $F_3(K)$ is equal to 119.25: an increase of more than a factor of three over the value of 36 for spheres. Eq. (34) reveals that for any given YSZ and LSM size distributions and volume fractions, L_{TPB} is directly proportional to $F_3(K)$. Thus, it can be concluded that for given volume fractions of

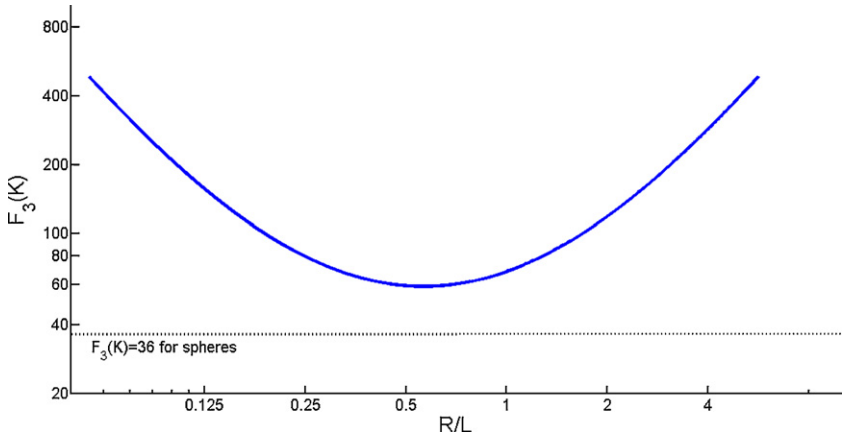

Fig. 3. Plot of $F_3(K)$ versus K.

the phases and particle size distributions, L_{TPB} depends significantly on the particle shape, and it is the lowest for spherical particles. *Therefore, changing the YSZ and LSM particle shapes from spherical to plate-like, or flake-like, or needle-like, can substantially increases* L_{TPB}. It is reported in the literature that at least LSM particles can be produced in a flake-like morphology [48]. Thus, the analysis brings an interesting opportunity to optimize L_{TPB} via a suitable choice of particle shapes.

4. Summary and conclusions

An analytical expression is derived for total triple phase boundary length per unit volume L_{TPB} in the microstructure of composite LSM/YSZ cathode. It is assumed that the microstructure is isotropic uniform-random and the microstrucutral volume of the composite cathode is at least of the size of the smallest representative volume element of the global microstructure, and there is no significant coarsening during the sintering process (which is reasonable for LSM/YSZ composite cathodes sintered below 1200 °C). The model explicitly brings out the effects of particle shapes, mean sizes, the coefficient of variation and the skewness of the size distributions, and volume fractions of YSZ, LSM, and porosity phases on L_{TPB}. The parametric analysis leads to the following conclusions.

1. L_{TPB} is the lowest when YSZ and LSM particles have spherical shape, and it can be substantially increased by using flake-like, plate-like, or needle-like YSZ and LSM particles.
2. Mono-size YSZ and LSM particle populations lead to higher L_{TPB} as compared to the populations having a distribution of sizes. Size distributions with large spread (high CV) can reduce the L_{TPB} by almost an order of magnitude. For a given CV, size distributions with negative skewness lead to a higher value of L_{TPB}.
3. For given relative proportion of YSZ and LSM, and given mean sizes, CV, and skewness of YSZ and LSM size distributions, the highest value of L_{TPB} is obtained at the *lowest* value of the porosity volume fraction that yields sufficient percolation and connectivity of pores for gas flow.
4. In the microstrucutral regime of interest for SOFC applications where all the three phases, LSM, YSZ, and porosity, must topologically percolate, the relative proportion of YSZ and LSM does not significantly affect L_{TPB}.

Acknowledgements

This research was supported through a grant from the U.S. National Science Foundation (grant DMR-0813630) for which Dr. B. MacDonald and Dr. A.J. Ardell are the Program Managers. The financial support is gratefully acknowledged. The views and conclusions contained herein are those of the authors and should not be interpreted as necessarily representing the policies or endorsements, either expressed or implied, of the funding agency.

References

[1] L. Carrette, K.A. Friedrich, U. Stimming, Chemphyschem 1 (2000) 162–193.
[2] R.M. Ormerod, Chem. Soc. Rev. 32 (2003) 17–28.
[3] V.A.C. Haanappel, J. Mertens, D. Rutenbeck, C. Tropartz, W. Herzhof, D. Sebold, F. Tietz, J. Power Sources 141 (2005) 216–226.
[4] V. Dusastre, J.A. Kilner, Solid State Ion. 126 (1999) 163–174.
[5] M.J. Jorgensen, M. Mogensen, J. Electrochem. Soc. 148 (2001) A433–A442.
[6] M. Juhl, S. Primdahl, C. Manon, M. Mogensen, J. Power Sources (1996) 173–181.
[7] E.P. Murray, S.A. Barnett, Solid State Ion. 143 (2001) 265–273.
[8] J. Fleig, Annu. Rev. Mater. Res. 33 (2003) 361–382.
[9] K. Sasaki, J.P. Wurth, R. Gschwend, M. Godickemeier, L.J. Gauckler, J. Electrochem. Soc. 143 (1996) 530–543.
[10] H.S. Song, W.H. Kim, S.H. Hyun, J. Moon, J. Electroceram. 17 (2006) 759–764.
[11] H.S. Song, W.H. Kim, S.H. Hyun, J. Moon, J. Kim, H.W. Lee, J. Power Sources 167 (2007) 258–264.
[12] M.J. Jorgensen, S. Primdahl, C. Bagger, M. Mogensen, Solid State Ion. 139 (2001) 1–11.
[13] Y. Ji, K. Yuan, J.N. Chung, J. Power Sources 165 (2007) 774–785.
[14] A. Abbaspour, K. Nandakumar, J.L. Luo, K.T. Chuang, J. Power Sources 161 (2006) 965–970.
[15] A. Ali, X. Wen, K. Nandakumar, J. Luo, K.T. Chuang, J. Power Sources 185 (2008) 961–966.
[16] D.G. Han, G.M. Choi, Solid State Ion. 106 (1998) 71–87.
[17] L.C.R. Schneider, C.L. Martin, Y. Bultel, D. Bouvard, E. Siebert, Electrochim. Acta 52 (2006) 314–324.
[18] P. Costamagna, P. Costa, E. Arato, Electrochim. Acta 43 (1998) 967–972.
[19] S. Sunde, J. Electrochem. Soc. 142 (1995) L50–L52.
[20] S. Sunde, J. Electrochem. Soc. 143 (1996) 1930–1939.
[21] S. Sunde, J. Electrochem. Soc. 143 (1996) 1123–1132.
[22] A. Tewari, A.M. Gokhale, R.M. German, Acta Mater. 47 (1999) 3721–3734.
[23] J. Ohser, F. Muecklich, Statistical Analysis of Microstructures in Material Science, J. Wiley & Sons, New York, 2000.
[24] L.A. Santalo, Integral Geometry and Geometric Probability, Mass. Addison-Wesley Publishing Co., Reading, 1976.
[25] D. Stoyan, S. Kendall, J. Mecke, Stochastic Geometry and its Applications, 2nd ed., John Wiley and Sons, NY, 1995.
[26] A.M. Gokhale, Quantitative Characterization and Representation of Global Microstructural Geometry, in: ASM Handbook: Metallography, and Microstructures. vol. 9, 2004, pp. 428–447.
[27] R.T. DeHoff, F.N. Rhines, Quantitative Microscopy, McGraw Hill Publishing Co., New York, NY, 1968.
[28] E.E. Underwood, Quantitative Stereology, Addison Wesley Publishing Co., Reading, Massachusetts, 1970.
[29] M.G. Kendall, P.A.P. Moran, Geometrical Probability, Hafner Publ., New York, 1963.
[30] M. Avrami, J. Chem. Phys. 7 (1939) 1103–1112.
[31] M. Avrami, J. Chem. Phys. 9 (1941) 177–184.
[32] W.A. Johnson, R.F. Mehl, Trans. Am. Inst. Min. Metall. Eng. 135 (1939) 416–442.
[33] H.K.D.H. Bhadeshia, Kinetics of simultaneous transformations, Solid-Solid Phase Transformations, in: International Conference on Solid-Solid Phase Transformation, 4th, Kyoto, Japan, May 24–28, 1999, pp. 1445–1452.
[34] S.J. Jones, H.K.D.H. Bhadeshia, Acta Mater. 45 (1997) 2911–2920.
[35] T. Kasuya, K. Ichikawa, M. Fuji, H.K.D.H. Bhadeshia, Mater. Sci. Technol. 15 (1999) 471–473.

[36] G. Matheron, Random Sets and Integral Geometry, Wiley, New York, 1974.
[37] J.L. Meijering, Philips Res. Reports 8 (1953) 270–290.
[38] R. Miles, On estimating aggregate and overall characteristics from thick sections by transmission microscopy, in: Fourth International Congresss for Stereology, NBS, Gaithersbug, Md., 1975, 3–12.
[39] C.S. Smith, L. Guttman, J. Met. 5 (1953) 81–87.
[40] E. Kreyszig, Advanced Engineering Mathematics, Wiley, 1998.
[41] W. Hays, Statistics, 4th ed., Holt McDougal, 1988.
[42] S. Sunde, J. Electroceram. 5 (2000) 153–182.
[43] R.T. DeHoff, Treatise on Materials Science and Technology, vol. 1, Academic Press, New York, NY, 1972, p. 247.
[44] A.M. Gokhale, C.V. Iswaran, R.T. DeHoff, Metall. Trans. A 11A (1980) 1377–1382.
[45] A.M. Gokhale, Metall. Trans. A 15A (1984) 243–245.
[46] J.R. Wilson, W. Kobsiriphat, W. Mendoza, H.-Y. Chen, J.M. Hiller, D.J. Miller, K. Thornton, P.W. Voorhees, S.B. Adler, S.A. Barnett, Nat. Mater. 5 (2006) 541–544.
[47] J. Wilson, A. Duong, J. Cronin, M. Gameiro, S. Rukes, K. H. Chen, D. Mumm, S. Barnett, "Structural and electrochemical characterization of $La_{0.8}Sr_{0.2}MnO_3$–Y_2O_3-stabilized ZrO_2 (LSM-YSZ) cathodes with varying composition," in *33rd International Conference & Exposition on Advanced Ceramics & Composites*, 2009.
[48] S.P. Jiang, J. Power Sources 124 (2003) 390–402.
[49] S. Zhang, M. Lynch, A.M. Gokhale, M. Liu, J. Power Sources 192 (2009) 367–371.
[50] C.W. Tanner, K.Z. Fung, A.V. Virkar, J. Electrochem. Soc. 144 (1997) 21–30.
[51] S. Zhang, A.M. Gokhale, Unpublished Research, Georgia Institute of Technology, 2008.